MESO Science & Nanotechnology

DOI: 10.64214/jmsn.01.03005 Proceedings

Josephson Transport through Spin-Orbit-Coupled $SrIrO_3$ and Sr_2IrO_4 Interlayers*

N. V. Dubitskiy,[1,2] G. A. Ovsyannikov,[1] Yu. V. Kislinskii,[1] G. D. Ulev,[1,3] A. M. Petrzhik[1]

[1] Kotelnikov Institute of Radio Engineering and Electronics, Russian Academy of Sciences, Moscow, Russia
[2] HSE University, Moscow, Russia
[3] Moscow Institute of Physics and Technology, Dolgoprudny, Russia

submitted 25 July 2026, accepted 30 August 2026, published 08 September 2026

The strontium iridate family includes both conducting and insulating phases with strong spin-orbit coupling. These materials can serve as interlayers in superconducting heterostructures. An epitaxial $SrIrO_3$ film grown on an $NdGaO_3$ substrate exhibited weakly nonmetallic resistivity and an approximately linear Hall response. A single-band analysis at 5 K yielded a carrier density of 2×10^{21} cm^{-3}, a resistivity of 6×10^{-3} Ω·cm, and a mobility of 0.6 cm^2/(V·s). We fabricated Nb/iridate/$YBa_2Cu_3O_{7-\delta}$ superconducting mesa heterostructures. For heterostructures containing 15-nm $SrIrO_3$ interlayers, I_cR_N was 0.1–0.3 μV at 4.2 K. The corresponding magnetic diffraction pattern had minima close to zero and a Fraunhofer-like central lobe. For 5-nm Sr_2IrO_4 interlayers, I_cR_N was 41–79 μV, and the area-normalized normal resistance was about two orders of magnitude larger than that of the $SrIrO_3$ devices. The R_NA ranges for heterostructures with $SrIrO_3$ and Sr_2IrO_4 interlayers were $(3-8) \times 10^{-8}$ and $(0.8-1) \times 10^{-5}$ Ω·cm^2, respectively. Resonant Fiske steps in the current–voltage characteristics corroborated ac Josephson dynamics.

Introduction

The Ruddlesden-Popper series $Sr_{n+1}Ir_nO_{3n+1}$ spans electronically distinct phases governed by comparable spin-orbit and correlation energy scales. The members considered here are the correlated paramagnetic semimetal $SrIrO_3$ and the spin-orbit-assisted antiferromagnetic insulator Sr_2IrO_4.[1] Spin-orbit coupling in superconducting hybrid structures can modify proximity-induced correlations and the current-phase relation, making strongly spin-orbit-coupled interlayers relevant to Josephson devices.[2] Josephson transport through strongly spin-orbit-coupled topological materials offers a related experimental precedent.[3]

Recent experiments on epitaxial $SrIrO_3$ have demonstrated that its semimetallic transport is sensitive to synthesis route, strain, disorder, and correlations.[4–8] In Sr_2IrO_4 thin films, the spin–orbit-entangled antiferromagnetic state is robust against substantial distortion, while the magnon spectrum remains sensitive to the electronic character of adjacent materials.[9,10] The contrast between these two phases allows a direct comparison of conducting and insulating weak links within a single iridate family.

Josephson coupling through $SrIrO_3$ was previously demonstrated in Nb/$SrIrO_3$/$YBa_2Cu_3O_{7-\delta}$ mesa heterostructures,[11] and Sr_2IrO_4 was subsequently examined as a higher-resistance interlayer.[12] The present extended abstract compares the film transport and heterostructure characteristics relevant to these two regimes. We focus on experimentally established observables: resistivity and Hall response, magnetic-field modulation of the critical current, area-normalized normal resistance, and resonant structures in the current-voltage characteristics ($I-V$ curves). Interpretations that would require phase-sensitive evidence for the microscopic pairing state are deliberately excluded.

Experimental details

Epitaxial $SrIrO_3$ and Sr_2IrO_4 films were grown on oxide single crystals by magnetron sputtering and pulsed-laser deposition under phase-selective temperature and oxygen-pressure conditions.[13–17] The representative transport sample was a 35-nm $SrIrO_3$ film grown on (110)$NdGaO_3$. Its resistivity was measured using the four-probe method, and its transverse Hall resistivity was recorded at 5 K in fields up to ±7 T (figure 1). The carrier density and mobility were evaluated within a single-band approximation.

The Josephson devices were fabricated on (110)$NdGaO_3$ as Nb/$SrIrO_3$/$YBa_2Cu_3O_{7-\delta}$ and Nb/Sr_2IrO_4/$YBa_2Cu_3O_{7-\delta}$ mesa heterostructures. Typical layer thicknesses were 60-70 nm for $YBa_2Cu_3O_{7-\delta}$, 100-200 nm for Nb, 15 nm for $SrIrO_3$, and 5 nm for Sr_2IrO_4. Mesa areas ranged from 10×10 to $50 \times 50\,\mu$m^2. The upper Nb electrode had a critical temperature of approximately 8.4 K; all junction data reported here were acquired at 4.2 K. The standalone transport film and the junction interlayers originated from related deposition runs. Consequently, the film data identify the conducting, strongly disordered $SrIrO_3$ regime but are not used as an exact parameterization of each weak link.

Results and discussion

Conducting $SrIrO_3$ interlayer

The resistivity increases only modestly upon cooling (figure 1), whereas the Hall response remains approximately linear over the measured magnetic field range. At 5 K,

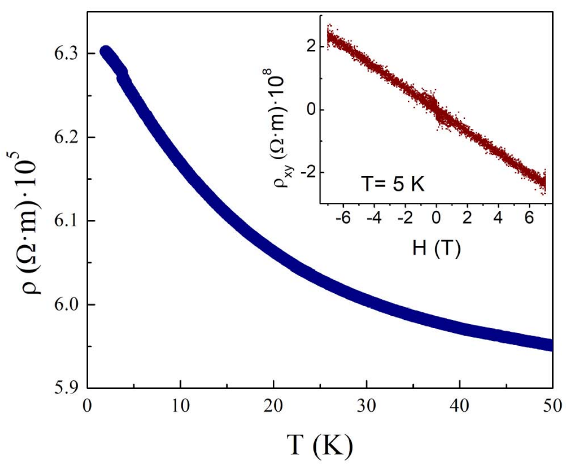

Figure 1. Temperature dependence of the resistivity of a 35-nm $SrIrO_3$ film grown on an $NdGaO_3$ substrate. The inset shows the transverse Hall resistivity at 5 K.

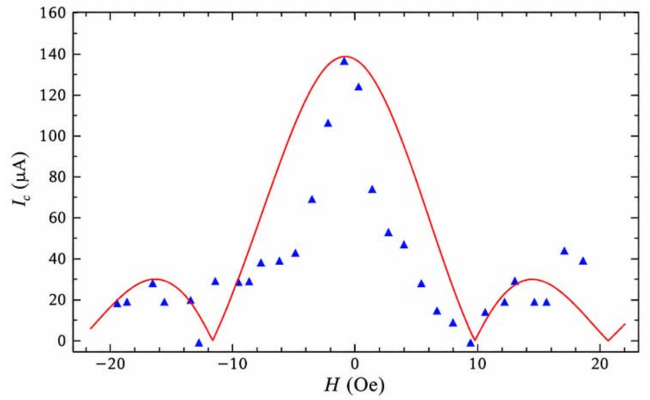

Figure 2. Magnetic-field dependence of the critical current for a $Nb/SrIrO_3/YBa_2Cu_3O_{7-\delta}$ junction at 4.2 K. Symbols are experimental data; the line is a Fraunhofer fit.

the single-band values were $n \simeq 1.8 \times 10^{21}\,\mathrm{cm}^{-3}$, $\rho \simeq 6.25 \times 10^{-3}\,\Omega\cdot\mathrm{cm}$, and $\mu \simeq 0.56\,\mathrm{cm}^2/(\mathrm{V\cdot s})$. These values place the film in a high-carrier-density, low-mobility regime. This behavior is consistent with the strong sensitivity of $SrIrO_3$ transport to synthesis, strain, disorder, and quantum corrections reported by independent groups and in our film series.[4–8,13–16,18] The weakly nonmetallic slope should therefore not be treated by itself as evidence for an excitation gap.

A $50\times50\,\mu\mathrm{m}^2$ junction with a 15-nm $SrIrO_3$ interlayer carried $I_c \simeq 140\,\mu\mathrm{A}$ and had $I_cR_N \simeq 0.1\,\mu\mathrm{V}$. The central part of $I_c(H)$ is described by the standard Fraunhofer expression with a maximum critical current $I_0 = 138.5\,\mu\mathrm{A}$, a magnetic field period $\Delta H_0 = 10.9\,\mathrm{Oe}$, a magnetic field shift $H_{\mathrm{off}} = 1.2\,\mathrm{Oe}$, and a negligible fitted background (figure 2).

The measured zero-voltage current is predominantly phase coherent. The offset is compatible with residual field or trapped flux, while the unequal side lobes can arise from current-density inhomogeneity, the in-plane lead geometry, and flux focusing.[19,20] The fit reproduces the central lobe and its first minima, the features most directly determined by the effective junction area. The residual deviations are therefore more naturally associated with a nonuniform spatial distribution of the supercurrent than with a loss of phase coherence. Similar nonideal diffraction patterns are common in finite-size junctions with nonuniform current density.[19,20]

With a current density $J_c \simeq 5.6\,\mathrm{A/cm}^2$ and an assumed magnetic thickness $d_{\mathrm{eff}} \simeq 250\,\mathrm{nm}$, the Josephson penetration depth is estimated as

$$\lambda_J = \sqrt{\frac{\Phi_0}{2\pi\,\mu_0\,d_{\mathrm{eff}}\,J_c}} \simeq 140\,\mu\mathrm{m}. \quad (1)$$

The resulting λ_J exceeds the $50\,\mu\mathrm{m}$ junction width. Self-field effects are therefore unlikely to be the dominant source of the observed asymmetry.

Insulating Sr_2IrO_4 interlayer

The 5-nm Sr_2IrO_4 interlayer produced a markedly different normal-state resistance scale while retaining Josephson coupling. For $40 \times 40\,\mu\mathrm{m}^2$ and $20 \times 20\,\mu\mathrm{m}^2$ devices, I_cR_N reached 41 and 79 μV, respectively. The magnetic diffraction pattern of the larger junction was fitted with a maximum critical current $I_0 = 64.2\,\mu\mathrm{A}$, a field period $\Delta H_0 = 3.32\,\mathrm{Oe}$, a magnetic field shift $H_{\mathrm{off}} = 0.05\,\mathrm{Oe}$, and a small background of approximately $1\,\mu\mathrm{A}$ (figure 3a). The current-voltage curves contain field-dependent resonant steps (figure 3b). These features are identified as Fiske steps, which result from resonant coupling of the ac Josephson oscillation to electromagnetic modes of the junction.[12,19,21] The area-normalized normal resistance R_NA of the Sr_2IrO_4 devices was approximately $9 \times 10^{-6}\,\Omega\cdot\mathrm{cm}^2$, about 200 times larger than that of the $SrIrO_3$ devices.

Together with the much larger I_cR_N, this contrast is consistent with two distinct weak-link regimes: a dissipative conducting interlayer for $SrIrO_3$ and a tunnel barrier for Sr_2IrO_4. Because the two device sets differ in interlayer thickness and fabrication details, the comparison is used to establish the transport regime rather than to extract a unique microscopic interface transparency.

Across the measured devices, I_cR_N ranged from $0.1-0.3\,\mu\mathrm{V}$ for $SrIrO_3$ and $41-79\,\mu\mathrm{V}$ for Sr_2IrO_4, while R_NA ranged from $(3-8)\times10^{-8}$ to $(0.8-1)\times10^{-5}\,\Omega\cdot\mathrm{cm}^2$, respectively. Thus, despite differences in geometry and interlayer thickness, both observables consistently distinguish the conducting and insulating weak-link regimes.

The small field offset and unequal side lobes in figure 3a should not be interpreted by themselves as evidence for an unconventional current–phase relation. As in the $SrIrO_3$ junction, residual field, flux focusing, and spatial variations of the current density can produce nonideal diffraction patterns.[19,20] The field-dependent resonant structure in Figure 3b provides an independent dynamical signature of Josephson coupling through its connection with cavity modes of the junction.[19,21]

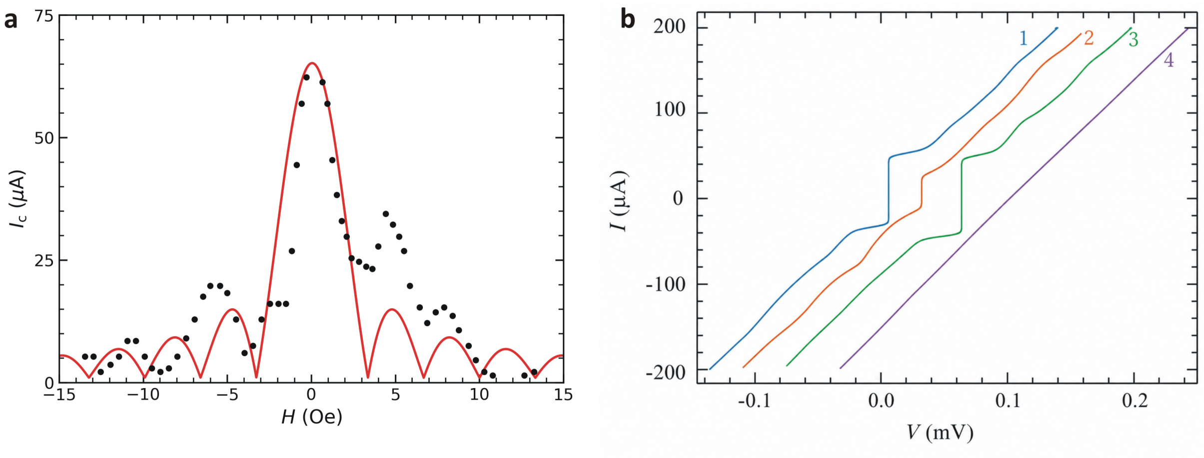

Figure 3. Nb/Sr_2IrO_4/$YBa_2Cu_3O_{7-\delta}$ junction: **a** – magnetic-field dependence of the critical current with experimental points and a Fraunhofer fit; **b** – I–V curves at $H = 0$ (1), +2.7 Oe (2), −2.5 Oe (3), and −9.6 Oe (4). The curves in panel b are shifted along the voltage axis for clarity.

Conclusion

Josephson transport was observed through both conducting $SrIrO_3$ and insulating Sr_2IrO_4 thin-film interlayers in Nb/iridate/$YBa_2Cu_3O_{7-\delta}$ mesa heterostructures. The $SrIrO_3$ interlayer combines high carrier density with low mobility and yields a low-voltage, strongly damped weak link. By contrast, the Sr_2IrO_4 interlayer increases both the characteristic voltage and the area-normalized normal resistance by about two orders of magnitude. The magnetic diffraction patterns confirm phase-coherent supercurrent; their asymmetries can be explained by residual or trapped flux.

Acknowledgements

The authors thank V. A. Baydikova, I. E. Moskal and K. E. Nagornykh for experimental assistance and useful discussions. This work is dedicated to the memory of Karen Y. Constantinian, a talented scientist, wise mentor, and remarkable person, whose contributions were essential to the development of this research. His scientific insight, profound knowledge, and dedication to science will always be remembered by his colleagues and students.

This study was carried out under State Assignment No. FFWZ-2025-0009 at the Kotelnikov Institute of Radio Engineering and Electronics of the Russian Academy of Sciences.

Contact information

Corresponding author: N. V. Dubitskiy,
orcid.org/0009-0003-1723-8103,
e-mail: nikita.dubitskiy@gmail.com

* Proceedings of the II International Scientific Conference "Advanced functional materials for digital and quantum electronics 2026", September 14–18, 2026, Dolgoprudny, Russia

References

[1] Moon S. J., Jin H., Kim K. W., Choi W. S., Lee Y. S., Yu J., Cao G., Sumi A., Funakubo H., Bernhard C., Noh T. W. *Dimensionality-controlled insulator-metal transition and correlated metallic state in 5d transition metal oxides* $Sr_{n+1}Ir_nO_{3n+1}$ *(*$n = 1, 2,$ *and* ∞*)*. Phys. Rev. Lett., vol. 101, no. 22, 226402 (2008).

[2] Amundsen M., Linder J., Robinson J. W. A., Žutić I., Banerjee N. *Colloquium: Spin-orbit effects in superconducting hybrid structures*. Rev. Mod. Phys., vol. 96, 021003 (2024).

[3] Stolyarov V. S., Yakovlev D. S., Kozlov S. N., Skryabina O. V., Lvov D. S., Gumarov A. I., Emelyanova O. V., Dzhumaev P. S., Shchetinin I. V., Hovhannisyan R. A., Egorov S. V., Kokotin A. M., Pogosov W. V., Ryazanov V. V., Kupriyanov M. Yu., Golubov A. A., Roditchev D. *Josephson current mediated by ballistic topological states in* $Bi_2Te_{2.3}Se_{0.7}$ *single nanocrystals*. Commun. Mater., vol. 1, 38 (2020).

[4] Choudhary R., Nair S., Yang Z., Lee D., Jalan B. *Semimetallic* $SrIrO_3$ *films using solid-source metal-organic molecular beam epitaxy*. APL Mater., vol. 10, 091118 (2022).

[5] Rimal G., Tasnim T., Calderon Ortiz G., Sterbinsky G. E., Hwang J., Comes R. B. *Strain-dependent insulating state and Kondo effect in epitaxial* $SrIrO_3$ *films*. Phys. Rev. Mater., vol. 8, L071201 (2024).

[6] Zhang Y., Pandey S., Ivanov S., Liu J., Urazhdin S. *Shot noise in a metal close to the Mott transition*. Nano Lett., vol. 24, 15943–15949 (2024).

[7] Fuchs D., Jaiswal A. K., Wilhelm F., Wang D., Rogalev A., Le Tacon M. *Robust spin-orbit coupling in semimetallic* $SrIrO_3$ *under hydrostatic pressure*. Phys. Rev. B, vol. 111, 075142 (2025).

[8] Paris E., Zhang W., Tseng Y., Efimenko A., Sahle C., Strocov V. N., Skoropata E., Rolfs K., Shang T., Lyu J., Pomjakushina E., Medarde M., Rønnow H.-M., Normand B., Radovic M., Schmitt T. *Coexistence of insulatorlike paramagnon and metallic spin-orbit exciton modes in* $SrIrO_3$. Phys. Rev. Lett., vol. 135, 186506 (2025).

[9] Shrestha S., Choi Y., Krautloher M., Zhu M., Hwang J., Keimer B., Seo A., Kim J.-W. *Exploring magnetic anisotropy and robustness of the* $J_{\text{eff}} = 1/2$ *state under*

substantial orthorhombic distortion in Sr_2IrO_4 thin films. Phys. Rev. B, vol. 109, 104415 (2024).

[10] Shrestha S., Souri M., Dietl C. J., Pärschke E. M., Krautloher M., Calderon Ortiz G. A., Minola M., Shi X., Boris A. V., Hwang J., Khaliullin G., Cao G., Keimer B., Kim J.-W., Kim J., Seo A. *Tunable magnons of an antiferromagnetic Mott insulator via interfacial metal-insulator transitions.* Nat. Commun., vol. 16, 3592 (2025).

[11] Petrzhik A. M., Constantinian K. Y., Ovsyannikov G. A., Zaitsev A. V., Shadrin A. V., Grishin A. S., Kislinskii Yu. V., Cristiani G., Logvenov G. *Superconducting current and low-energy states in a mesa-heterostructure interlayered with a strontium iridate film with strong spin-orbit interaction.* Phys. Rev. B, vol. 100, 024501 (2019).

[12] Kislinskii Yu. V., Constantinian K. Y., Moskal I. E., Dubitskiy N. V., Petrzhik A. M., Shadrin A. V., Ovsyannikov G. A. *Strontium iridates as barrier materials for Josephson heterostructures.* Russ. Microelectron., vol. 52 (Suppl. 1), S53–S58 (2023).

[13] Dubitskiy N. V., Baydikova V. A., Ovsyannikov G. A., Moskal I. E., Petrzhik A. M., Shadrin A. V. *Epitaxial growth, structure and electronic transport of $SrIrO_3$ thin films.* Radioelectronics. Nanosystems. Information Technologies, vol. 17, 439-448 (2025).

[14] Dubitskiy N. V., Baydikova V. A., Petrzhik A. M., Moskal I. E., Shadrin A. V., Shmakov V. A., Ovsyannikov G. A. *Structure and electronic transport in $SrIrO_3$ thin films under epitaxial strain induced by substrate lattice mismatch.* Phys. Solid State, vol. 67, 1073-1081 (2025).

[15] Moskal I. E., Petrzhik A. M., Kislinskii Yu. V., Shadrin A. V., Ovsyannikov G. A., Dubitskiy N. V. *Production of and electronic transport in thin films of strontium iridate.* Bull. Russ. Acad. Sci. Phys., vol. 88, 582-585 (2024).

[16] Baydikova V. A., Dubitskiy N. V., Petrzhik A. M., Ovsyannikov G. A., Moskal I. E., Shadrin A. V., Nagornykh K. E. *Effect of epitaxial stresses on the structure and electron transport in strontium iridate thin films.* Phys. Met. Metallogr., vol. 126, 1652-1658 (2025).

[17] Moskal I. E., Kislinskii Yu. V., Petrzhik A. M., Ovsyannikov G. A., Dubitskiy N. V. *Growth of epitaxial thin films of Sr_2IrO_4 antiferromagnet for spintronic heterostructures.* Phys. Solid State, vol. 66, 1063-1067 (2024).

[18] Danilyuk A. L., Podryabinkin D. A., Filonov A. B., Ovsyannikov G. A., Ulev G. D., Constantinian K. Y., Migas D. B. *Role of quantum contributions in the magnetoconductance behavior of iridate films at low temperatures.* Phys. Chem. Chem. Phys., vol. 28, 1357-1367 (2026).

[19] Barone A., Paternò G. *Physics and Applications of the Josephson Effect.* Wiley, New York, 1982.

[20] Suominen H. J., Danon J., Kjaergaard M., Flensberg K., Shabani J., Palmstrøm C. J., Nichele F., Marcus C. M. *Anomalous Fraunhofer interference in epitaxial superconductor-semiconductor Josephson junctions.* Phys. Rev. B, vol. 95, 035307 (2017).

[21] Coon D. D., Fiske M. D. *Josephson ac and step structure in the supercurrent tunneling characteristic.* Phys. Rev., vol. 138, A744–A748 (1965).